Fusion Engineering and Design 204 (2024) 114518

Contents lists available at ScienceDirect

Fusion Engineering and Design

journal homepage: www.elsevier.com/locate/fusengdes

Re-design of EU DEMO with a low aspect ratio

C. Bachmann [a,b,*], M. Siccinio [a,c], A. Ciula [d], P. Fanelli [d], G. Federici [a], L. Giannini [a], C. Luongo [a], P. Pereslavtsev [e], X. Sarasola [f], T. Steinbacher [a], H. Zohm [a,c]

[a] EUROfusion Consortium, FTD Department, Boltzmannstr. 2, Garching, Germany
[b] Technical University of Denmark, Lyngby, Denmark
[c] Max Planck Institute for Plasma Physics, Garching, Germany
[d] DEIm Department, University of Tuscia, Largo dell'Universitá, Viterbo 01100, Italy
[e] Association KIT-Euratom, Karlsruhe Institute of Technology (KIT), Karlsruhe, Germany
[f] École Polytechnique Fédérale de Lausanne (EPFL), Swiss Plasma Center, (SPC), PSI, Villigen CH-5232, Switzerland

ARTICLE INFO

Keywords:
DEMO
Tokamak
Aspect ratio
Magnetic field

ABSTRACT

The design point that had been chosen for EU DEMO in 2016 is reviewed here and a modification is proposed with a lower aspect ratio. Previously the same aspect ratio, A, was chosen for EU DEMO as in major tokamak experiments including ITER (A = 3.1), and, to rely on mature technology, a peak magnetic field no greater than 13 T was considered. Here we do not consider these limitations recognizing the recent commissioning of JT60-SA with A = 2.5 and the successful recent operation of a model coil at a field of >20 T.

EU DEMO must have a burning plasma and meet performance requirements relevant to a fusion power plant - at present, 2 GW fusion power and 2 h pulse length. The better plasma confinement at higher magnetic field allows reaching this condition in a smaller plasma. Thus, increasing the magnetic field appears as an obvious strategy to reduce the machine size. We confirmed though previous observations that the choice of a high magnetic field is associated with a large aspect ratio, mainly to generate space for the larger TF coils. In practice the magnetic field strength on DEMO-size TF coils is limited to ~12 T by the high electromagnetic loads. Also, the extreme heat flux on the divertor increases further with the magnetic field. Hence the magnetic field on the plasma axis is limited in EU DEMO to ~5.4 T, its aspect ratio to approximately 3.

The limiting factor to lowering the aspect ratio is the space on the inboard side. This is primarily driven by the requirement to integrate the central solenoid to drive the plasma current inductively. Our literature review suggests that non-inductive plasma scenarios, as considered in most power plant studies in literature, are optimistic and not sufficiently supported by experimental results. Also, the space required for the superconducting toroidal field coils, the tritium breeding blanket, and the neutron shield is substantial. For a DEMO device the space on the inboard side becomes insufficient for aspect ratios below ~2.6. We therefore conclude the aspect ratio of EU DEMO should be chosen within the range ~2.6 - ~3.0 trading-off lower magnetic field and lower divertor heat loads against machine compactness.

1. Introduction

1.1. Basis for a re-definition of the DEMO design point

EU DEMO is the step between ITER and a commercial fusion power plant [1–3]. It shall convert the heat generated in the plasma chamber into electricity delivering a few hundred MWs into the grid and operate with a closed tritium fuel cycle. It shall also adopt concepts of plasma physics, control and operation, technologies and design that are directly relevant or could be extrapolated to the construction and operation of a fusion power plant.

In 2016 a reference configuration of EU DEMO was chosen as a basis for the design and physics development in the DEMO pre-conceptual design phase [4]. As in ITER, Nb_3Sn was considered in 2016 as conductor material for the toroidal field (TF) coils given the "low extrapolation" approach to minimize technological risks [3]. EU DEMO was defined as a machine with a major radius $R \sim 9\,m$, an ITER-like field of ~12 T on the conductor and the ITER aspect ratio of 3.1. The

* Corresponding author at: EUROfusion Consortium, FTD Department, Boltzmannstr. 2, Garching, Germany.
E-mail address: christian.bachmann@euro-fusion.org (C. Bachmann).

https://doi.org/10.1016/j.fusengdes.2024.114518
Received 8 December 2023; Received in revised form 14 May 2024; Accepted 19 May 2024
Available online 28 May 2024

following are key issues of the chosen configuration:

(i) Its associated plant systems will have substantial costs since it is significantly larger than ITER .
(ii) The manufacturing difficulty of the associated large DEMO TF coils [5].
(iii) The high power carried by charged particles across the separatrix to the divertor [3].

In this article we revisit the 2016 reference configuration assessing the impact of two design parameters: the *magnetic field* strength and the plasma *aspect ratio*:

At a higher magnetic field, the confinement of the plasma energy increases, which is therefore desirable as a basic principle to increase the performance. High-temperature superconductor (HTS) technologies such as REBCO [6] that offer the potential to increase the magnetic field on the conductor to 20 T and more were previously not considered for DEMO. It is, however, considered elsewhere [7–9]. To the contrary, given the difficulties and cost associated with building high-field coils, the advantages of reducing rather than increasing the magnetic field are highlighted in [10] and [11]. In this article we determine DEMO design points sizing the main tokamak components with simple formulae for a large range of the magnetic field and of the aspect ratio.

The aspect ratio, A, is defined as the ratio between the plasma major radius R and its minor radius a. Plasmas with smaller A have three important advantages:

i. As the torus geometry approaches that of a sphere, such tokamaks tend to become more compact, which is typically considered favorable since size is a major cost driver.
ii. At a given magnetic field a plasma with a smaller aspect ratio can be confined at higher pressure. The reason is the higher plasma current at low A at a given safety factor, q_{95}. This, together with an increase in volume, allows for efficient confinement even in low fields. As a side effect, the value of the normalized pressure, β_N, increases, [12], which may impact on the global plasma stability.
iii. Plasmas with lower aspect ratio have a larger natural elongation κ, i.e., the ratio of its vertical to its radial diameter [13]. A higher plasma elongation increases the fusion power significantly since it allows for both an increase in plasma volume and for higher currents at given q_{95}.

In fact, JET had first been devised in the 1970s with a low aspect ratio of $A = 2.4$ and compact inboard magnet mechanical structures, [14]. During the installation of the JET divertor in 1993, the aspect ratio was increased to $A = 3.1$ [15]. Also, DIII-D and later JT60-SA were designed with a compact machine build, both with $A = 2.5$.

Although in 2016 the impact of A on the DEMO machine was assessed regarding several aspects, a "conventional" aspect ratio of $A = 3.1$ was chosen mainly based on the fact that the physics basis is best developed for machines with aspect ratios of ~3 [4], e.g., from JET and ASDEX-Upgrade, see Table 1. In the early 90s the same reasoning led to the choice of $A = 3$ for the NET tokamak: "*The aspect ratio of the NET plasma was taken to be A = 3. This choice minimizes the uncertainties in predicting the confinement properties of the plasma as present large tokamaks all have aspect ratios around this value.*", [16], and also for ITER: "*the lack of aspect ratio variation in the data…led to a choice of an aspect ratio close to that of the major tokamak experiments (A = 3) to minimize the physics risk.*", [17].

1.2. DEMO performance requirements

The performance requirements of EU DEMO have a strong impact on the design point. These are described below, summarized in Table 2, and are in line with the considerations made in the European Power Plant Conceptual Study (PPCS) [36] and European Roadmap to Fusion Electricity [1].

Table 1
Major and minor radii, aspect ratio and plasma elongation of existing and *planned* tokamak machines operating high performance plasma modes such as the H-mode in divertor configuration and hence with high relevance for the ITER and DEMO physics basis, see also [18]. Sorted roughly by aspect ratio. Note: values vary to some degree in different campaigns.

	R_0	a	A	κ_{95}
MAST-U [19]	0.85 m	1.23 m	~1.5	2.0
NSTX-U [20]	0.93 m	0.55 m	1.7	2.3
T-15MD [21]	1.48 m	0.67 m	2.2	
JT60-SA [22]	2.96 m	1.18 m	2.5	1.95
DIII-D [23]	1.66 m	0.67 m	2.5	≤ 2
JET [15]	2.96 m	0.95 m	3.0	1.85
DEMO low A	*8.0 m*	*2.85 m*	*2.8*	*1.74*
DEMO 2016 [24]	*9.1 m*	*2.9 m*	*3.1*	*1.59*
CFETR [25]	*7.2 m*	*2.2 m*	*3.3*	*2.0*
ITER [26]	*6.2 m*	*2.0 m*	*3.1*	*1.7*
ITER 1996 [27]	*8.1 m*	*3.0 m*	*2.7*	*1.6*
JFT-2M [28]	1.3 m	0.35 m	3.7	1.7
JT-60U [29]	~3.3 m	1.1 m	3.1	1.2-1.8
SPARC [30]	1.9 m	0.57 m m	3.3	1.97
DTT [18]	2.15 m	0.65 m	3.3	1.66
ASDEX-U [31]	1.625 m	0.5 m	3.25	1.6
TCV [32]	0.88 m	0.25 m	3.52	>2
KSTAR [33]	1.8 m	0.5 m	3.6	2.0
EAST [34]	1.7 m	0.4 m	4.25	1.6-2.0
WEST [35]	2.5 m	0.5 m	5.0	1.3-1.6

Table 2
DEMO performance requirements.

Perform. requirement	Associated value
Lifetime neutron fluence	70 dpa ≡ 6 fpy
Fusion power	2000 MW
Power density	avg. neutron wall load (NWL) ≥1.0 MW/m^2
Pulse length	2.0 h
Tritium self-sufficiency	Breeding blanket installed on inboard and outboard side

A **reliable plasma regime of operation** is considered as close as possible to the ITER Q = 10 baseline scenario, in order to minimize the extrapolation risks [37,38]. The main features are:

- Plasma energy confinement time assumed in line with the predictions of the IPB98(y,2) scaling i.e., H = 1.0 [39].
- Plasma current driven mainly inductively.
- The 0D stability criteria from experimental experience fulfilled ($q_{95} > 3$, $\beta_N < 3.5$, Greenwald density limit).

The first and third criterion are speculative to some extent, i.e., they assume DEMO to operate "as expected" based on current experimental results on smaller machines but are not based on a first-principle demonstration. New results, in particular from ITER, might require their modification. The main difference of the DEMO scenario as compared to that of ITER is the use of seeded impurities [40] to enhance the core radiation in order to reduce the power crossing the separatrix, P_{sep}, up to $\sim P_{LH}$, where P_{LH} is the L-H threshold power calculated with the Martin scaling [41]. Currently, there is a debate inside the plasma physics community about the validity of applying this scaling to reactor-size devices like ITER or DEMO. Indeed, other scaling laws have been proposed, which seem to better reproduce the behavior of high-power JET shots [42]. However, since most of the worldwide fusion reactor designs, including the 2016 EU DEMO, are based on the Martin scaling, we retain this convention for consistency. The condition $P_{sep} > P_{LH}$ has to be fulfilled in order to ensure H-mode and the corresponding high energy confinement time. However, this assumption has the important consequence of *linking P_{sep} to the magnetic field strength*

(which P_{LH} depends on), which has relevant implications on our results, see Section 4.2. Some of the aspects listed above are discussed in more detail in the following paragraphs.

Since DEMO shall play the role of a *Component Test Facility* and demonstrate materials suitable for a **high lifetime neutron fluence,** [1], it must generate an accumulated lifetime neutron fluence of few MW year/m^2 that corresponds to a damage level in the wall materials of 20 + 50 displacements per atom (dpa) [2].

The target for the **net electric output** of the DEMO plant is defined in [1] as "*hundreds of MW of electricity*". With common assumptions regarding the heat conversion efficiency and recirculating power for various DEMO systems, this translates into a requirement for the fusion power of $P_{fus} = \sim 2000$ MW, which corresponds to a net electricity output of 400–500 MW, see also [2] and [3]. Furthermore, a requirement for the power density must be considered. In a fusion reactor, in contrast to a fission reactor, the heat is removed in the reactor walls rather than inside the volume of a pressure vessel. We therefore consider the power density requirement as a surface power flux [MW/m^2] rather than a volumetric power generation [MW/m^3]. This is represented by the average $NWL = 80\ \% P_{fus} / A_{Wall}$, with A_{wall} being the surface area of the plasma-facing wall. Too low values of the *NWL* correspond to an unattractively large device with respect to the produced fusion power. We consider a *NWL* target of ~1 MW/m^2 as reasonable, which lays in between the ITER target of 0.57 MW/m^2 [26] and ~2 MW/m^2 as considered for fusion power plants in the PPCS [36].

The **pulse length** of a given device can be extended mainly by increasing the radial size of the central solenoid, which would lead to an increased major radius. For a shorter pulse length, driving the plasma current requires less magnetic flux but a larger number of pulses is needed to reach the target lifetime neutron fluence. In fact, below a pulse length of ~0.5 h fatigue limits lead to an *increase* in the size of the central solenoid (CS) despite the reduced flux requirement [43]. In this DEMO design point study, a pulse length of 2 h has been chosen as considered also in [3].

The **tritium self-sufficiency** of DEMO as required by the European roadmap requires the integration of a breeding blanket (BB) around the plasma whose size impacts the radial build of the machine. The remainder of the paper is organized as follows: Section 2 of this article includes a literature review of fusion power plant studies, Section 3 describes the system code study to identify potential DEMO design points, and Section 4 provides assessments of the identified DEMO design points.

2. Power plant studies in literature

2.1. Pulsed vs. steady-state plasma operation

Tokamaks in contrast to stellarators were initially considered as intrinsically pulsed devices because their plasma current was assumed to be driven inductively by discharging the poloidal field (PF) coils and, in particular, the CS. The need for energy storage to provide steady-state power output and also fatigue of reactor components were seen as major issues of pulsed fusion power plants [44]. In the 1980s major milestones in fusion research were reached through the successful operation of e.g., JET, TFTR, and of JT60 [45]. It was then considered to replace the inherently pulsed inductive current drive by maximizing the so-called bootstrap current and by employing auxiliary systems driving the remaining part of the plasma current, as explained in the next sections.

2.1.1. Bootstrap current

The bootstrap current [46] that drives a fraction of the plasma current is known since the early 70s [47] and was found to be substantial in TFTR [48]. It is known from plasma physics that the bootstrap current increases with increasing plasma pressure, or more precisely with higher poloidal-beta, β_{pol}, values [49], where $\beta_{pol} \sim p/I_p^2$, with p being the plasma pressure, and I_p the plasma current. However, to avoid magnetohydrodynamic (MHD) instabilities such as Resistive Wall Modes (RWM), β_{pol} must be limited. For this reason, even if the confinement was better (i.e., H > 1) and thus a high plasma pressure could be achieved at low current, the margin for reducing the current was limited by stability considerations. An enhanced confinement at lower current is obtained in existing tokamak experiments via an active, accurate tailoring of the safety factor profiles by auxiliary plasma heating systems. However, it appears challenging to realize this approach in a burning plasma whose heating (and thus β_{pol}) is dominated by the alpha particle population rather than by auxiliary heating systems. The large fluctuation of the alpha particle heating can be expected to prevent any accurate tailoring of the safety factor profiles since large fluctuations in the plasma pressure (locally) lead to corresponding fluctuations in the (local) bootstrap current profile, which are challenging and expensive to control. Thus, the MHD stability effectively limits the achievable *fraction* of the plasma current provided by the bootstrap current, f_{BS}, and this is not much affected by the aspect ratio, see also Section 3.6. The highest bootstrap current fraction we found in literature is reported for long pulse experiments conducted at EAST (A = 4.25) as ~50 % [50]. Research at NSTX ($A = 1.7$) leads Menard et al. to suggest that achieving bootstrap current fractions greater than 50 % cannot be realistically expected in future spherical tokamaks [51]. Nonetheless, hopes on higher bootstrap current fractions are set e.g., in the Japanese A-SSTR2 study ($f_{BS} = 83$ %) and at Tokamak Energy[1] where it is counted on an f_{BS} of 95 % [52] or even 100 % [53]. The scenarios considered in this work are not designed to maximize the bootstrap current i.e., no active tailoring of the safety factor profile nor any confinement enhancement is assumed.

2.1.2. Auxiliary current drive

For steady-state plasma operation in tokamaks in addition to the bootstrap current, auxiliary current drive systems are required to drive part of the plasma current, e.g., lower hybrid, electron cyclotron, ion cyclotron and neutral beam injection. High non-inductive current fractions were achieved in this way e.g., in JFT-2M [28], in Triam-1M [54], Tore Supra [55], SST1 [56], NSTX-U [51], EAST [50], and ASDEX Upgrade [57]. It is conceivable that with a large amount of installed auxiliary current drive power fully non-inductive current drive can be achieved. However, the power consumption of these auxiliary systems is high. A typical value for current drive efficiency is 1 MA per 20 MW coupled to the plasma, which corresponds to ~50 MW electricity consumption [58]. To drive the plasma current in a DEMO-like device by auxiliary systems an excessive amount of auxiliary current drive power would be required [59,36,37]. Relying on auxiliary systems to drive the plasma current is for this reason generally seen as incompatible with a power plant [60].

2.1.3. Pulsed next step devices

The steady-state operation of fusion power plants would be desirable. Exploring fully non-inductive plasma scenarios has therefore been defined as one of ITER's missions [26,61]. Also, JT60-SA aims at exploring plasma scenarios with high bootstrap current [22]. In such scenarios the plasma current, I_p, is typically reduced. This has the twofold purpose of (i) achieving a high β_{pol}, (which is proportional to $1/I_p$) to maximize the bootstrap current fraction [62], and (ii) to minimize the remaining part of the plasma current required to be driven by the auxiliary heating systems. The ITER non-inductive baseline scenario foresees in fact a plasma current of only 9 MA, well below that foreseen for the inductive Q = 10 scenario with I_p = 15 MA, [61]. Since high plasma currents are normally required to obtain a sufficiently high fusion power gain, low-current scenarios must rely on an improved plasma confinement (H-factor > 1). The ITER non-inductive baseline

[1] www.tokamakenergy.com

scenario targets $H = 1.6$, CFETR, which targets a steady-state operation, aims at $H = 1.12 - 1.42$ [25]. Campbell et al point out that substantial research will be required, in particular in ITER, to identify a plasma scenario suitable for non-inductive operation, the outcome of which is open [61]. For EU DEMO this route has been discontinued but will be reconsidered in case new research results allow the definition of a credible non-inductive plasma scenario [63]. Inductive plasma scenarios were therefore considered in ITER's predecessors INTOR [64] and NET [16], and are considered in ITER itself, in SPARC [65], in the DEMO reactor developed in Japan [66], and also for EU DEMO.

If non-inductive scenarios are discarded, a CS must be integrated in the machine design to provide the magnetic flux required to drive the plasma current. The large size of such a CS has a major impact on the machine major radius and also defines a lower limit to the choice of the aspect ratio. The main basis of tokamak reactor studies proposing more compact machines with low aspect ratio is the assumption the plasma current could be driven non-inductively, often relying on high β_{pol} values, see Table 3.

2.2. Impact of A on the design of tokamaks

2.2.1. Spherical tokamaks

Spherical tokamaks with $A < 2$ offer the most compact machine configuration and several fusion power plant studies considering such designs predict attractive performance, e.g. [83,72,52]. These reactors benefit to a high degree from the advantages associated with a low aspect ratio listed above. Their main issue, as recognized already in 1998 [84], is the limited space on the inboard side [85]. The location of the TF coil inboard leg in a spherical tokamak close to the machine center implies the toroidal width of the coils is small, limiting the space for the winding pack. The same applies for the mechanical structures required to resist its electromagnetic (EM) forces. This issue is reflected by the rather low fields on axis in the main spherical tokamak experiments, NSTX (0.44 T before and 0.63 T after the upgrade [20]) and MAST (0.52 T before and 0.78 T after the upgrade [19]). During the JET design phase (3.6 T [15]) significant efforts were made to minimize the aspect ratio, yet it could not be reduced below 2.4 [14].

Since there is hardly any space for the CS in a spherical tokamak, across all reactor studies the CS is not considered to provide inductive current drive to maintain the plasma current, see Table 3. For the magnetic flux required for the plasma breakdown and ramp-up several alternative concepts are proposed in literature: a slim solenoid providing a minimum magnetic flux [85], using the external PF coils [86], and the merging-compression method that relies on large coils inside the plasma chamber on the outboard side, which the plasma is moved away from during flat top [87]. The latter is not applicable to fusion machines that generate any significant level of neutron fluence, which makes the integration and maintenance of coils facing the plasma infeasible, e.g., due to excessive heat loads and the unavailability of electrical insulation materials.

The fact that so far plasma current ramp-up concepts without CS lack validation, and non-inductive plasma scenarios have not been substantiated (especially concerning the active control of safety factor profiles in a highly fluctuating plasma dominated by alpha heating) leads to the conclusion that the design of EU DEMO as a spherical tokamak is not a suitable choice.

Table 3
Overview of selected tokamak reactor studies

Study	Year	Current drive	A	R_0	B_0 [T]
CIT [67]	1987	ind.	2.7	1.2 m	10.5
NET [16]	1993	ind.	3.0	7.3 m	5.2
PPCS-B [36]	2006	ind.	3.0	8.6 m	6.9
INTOR [64]	1981	ind. + aux	4.0	5.2 m	5.5
STARFIRE [68]	1981	non-ind.	3.6	7.0 m	5.8
Tiber-II [69] [70]	1987	non-ind.	3.6	3.0 m	6.0
ARIES-I [71]	1991	non-ind.	4.5	6.8 m	11.3
ARIES-ST [72]	2003	non-ind.	1.6	3.2 m	2.1
ARIES-AT [73]	2006	non-ind.	4.0	5.2 m	5.8
FIRE [74]	2000	non-ind.	3.8	2.0 m	10.0
FNSF [75]	2018	non-ind.	4.0	4.8m	7.5
FNSF-ST [76]	2011	non-ind.	1.6	1.3m	
ARC [77]	2015	non-ind.	2.9	3.3 m	9.2
UK-ST [52]	2002	non-ind.	1.4	3.4 m	?
UK-ST135 [78]	2018	non-ind.	1.8	3.5	3.7
SSTR [79]	1990	non-ind.	4.1	9.0 m	7.3
A-SSTR2 [80]	2002	non-ind.	4.1	6.2 m	11.0
VECTOR [81]	2003	non-ind.	2.0	3.8 m	5.0
SlimCS [82]	2007	non-ind.	2.6	5.5 m	6.0

2.2.2. Tokamaks with high aspect ratio

At higher A the reduction of the plasma minor radius increases the available space on the inboard side and allows integrating larger TF coils to generate a higher magnetic field. When operated in a higher magnetic field the same fusion power can be generated in a smaller plasma because of the higher confinement capability and energy density. This is an obvious path to more compact and potentially cheaper fusion reactors e.g., the different ARIES studies from 1991 to 2006 were devised with high magnetic field and aspect ratios of ~4 [73]. That approach is still followed in today's reactor studies [77,85]. However, the difficult engineering of high-field magnets subject to very high EM loads is recognized in several studies of compact reactors and ultimately also imposes a limit as to how compact a machine can actually be made [85, 88,11].

3. Input and procedure to identify DEMO design points

3.1. Overview

There are no known hard boundaries within the range of aspect ratios where plasma characteristic values such as beta or elongation would display a sharp drop or rise [89,90]. Instead, they change smoothly with A, and we have implemented dependencies on A that we postulate in a system code. These are described in this chapter.

The system code was used to identify DEMO design points across a wide range of aspect ratio values with self-consistent plasma parameters and realistic sizing of the main tokamak components. The system code that sizes the tokamak components is coupled to PLASMOD [91], a simplified steady-state transport code based on ASTRA [92]. It considers the input values provided in Table 4, and sizes the plasma and the tokamak components on the inboard side. In the table, n_{GW} indicates the Greenwald density, i.e., the empirical limit density achievable in a tokamak.

$$n_{GW}\ \left[1e20m^{-3}\right] = \frac{I_p\ [MA]}{\pi a^2}$$

Note that assuming a constant Greenwald fraction links the density, and therefore the fusion power, to the plasma current, I_p, and to the minor radius, a. The system code is run iteratively, varying the magnetic field, and checking the radial build consistency, aiming at the most compact radial build.

Table 4
Values of important parameters used in this design point study.

Parameter	Value
Confinement, H	1.0
Safety factor, q_{95}	3.5
Plasma triangularity, δ	0.3
normalized β_N	<3.5
Pedestal top density	$0.85^{*}n_{GW}$
Auxiliary heating used for plasma current drive, see section 3.7	50 MW
Von Mises stress limit in TF coil inboard leg	660 MPa
Distance TF coil – plasma (inboard)	1.6 m

3.2. Optimization with respect to cost and size

Improving the economics of DEMO or future fusion devices is essential since the predicted figures for the cost of electricity are higher than those of conventional power plants [36]. Both the capital as well as the operational costs need to be considered [93]. The most expensive components of a DEMO or fusion power plant are expected to be the superconducting magnetic coils, the plasma-facing in-vessel components (IVCs) i.e., the breeding blanket and the divertor, as well as the nuclear buildings, see also Section 4.5. These main cost factors all depend on the size of the IVCs e.g., the size of the large structures, installations and transfer corridors required for their replacement [94] scale with their size affecting the plant capital cost. Also, the significant cost of the infrastructure required for the treatment and storage of IVCs as nuclear waste depends on their size [95,96]. The main cost items are therefore linked more directly to the plasma surface area, A_{pl}, than to the major radius. Hence A_{pl} is used here as a first order figure to represent the size and hence the cost of DEMO.

3.3. Plasma triangularity

In general, low A values allow for higher triangularities since the relative distance between plasma and PF coils is smaller due to the larger plasma minor radius. However, the optimal value for the triangularity is the result of a number of optimizations, like the constraints on the divertor geometry or the choice of the confinement regime (which in DEMO will not necessarily be a type-I Edge-Localized mode (ELMy) H-mode, but rather a small- or no ELM-regime [38]). For this reason, and because the pedestal top density is fixed in any case, the role of the triangularity is minor in this analysis and has been kept constant at 0.3.

3.4. Plasma elongation

Plasmas with lower aspect ratio have a higher natural elongation and offer more margin regarding the plasma vertical stability, which is partly due to the smaller relative distance between plasma and passive structure and control coils [90]. This allows operating a D-shape plasma with a small increase of its elongation, which leads to a notable increase of the fusion power, [97]. This fact was not fully understood in the 1980s and therefore neither considered in the STARFIRE power plant studies [98] nor in the initial definition of the ITER concept [17]. We found the first assessment of the plasma elongation considering the controllability of the plasma in [99], which finds a negligible dependence of the controllable plasma elongation with the lower aspect ratio due to the simplified assumptions made at the time. Later studies found a stronger dependence [97], which is considered here (since q_{95} is fixed and the density is linked, via the Greenwald limit, to the plasma current, which can be increased at high elongation). In this design point study, the plasma elongation, k_{95}, has been maximized to the limit of vertical stability control. The consequent k_{95} values shown in Table 5 reflect the higher natural plasma elongation at lower aspect ratio. Notably, the limit elongation values we consider are much lower than those identified in [99].

3.5. Normalized beta, β_N

A high β_N is an indication of good plasma performance, since it reflects the capability of achieving a high plasma pressure at low "cost" (plasma current and field). However, two limits are often defined for the normalized β_N, [100]:

- Above the so-called "no-wall limit" the plasma is unstable against RWM, which are instabilities developing on a slow time scale. If an active control is present e.g., in-vessel coils, these modes can be stabilized, and the plasma be operated even if β_N exceeds the limit.
- Above the so-called "ideal wall limit", at very high β_N, the plasma becomes unstable on MHD timescales (fractions of milliseconds) and is therefore not controllable.

This means that, if one can keep RWMs under control, the discharge can be run at higher β_N with robust margins against disruptions and achieving a better plasma performance [72,78,82]. In this paper, however, we only consider plasmas which are stable w.r.t. the more stringent no-wall limit. In fact, we consider an additional requirement for active RWM control an overcomplication for the machine design and operation.

Table 5
Plasma elongation, k_{95}, considered in this study.

A	2.4	2.6	2.8	3.1	3.3	4.0	4.5
k_{95}	1.92	1.80	1.74	1.65	1.62	1.45	1.38

3.6. Bootstrap current

All design points determined in this work assume pulsed devices, relying on a substantial fraction of the plasma current to be driven inductively. The fraction of bootstrap current, f_{BS}, amounts to ~39 % at low A and ~30 % at high A, i.e., no major variation across the parameter space that would allow the consideration of a steady-state plasma, see also Section 2.1.1 above. The bootstrap current density (i.e., per unit surface) tends to be higher at low aspect ratio since the fraction of trapped particles in the plasma is higher. At the same time, however, low-A machines are operated with a larger current in absolute terms, thus the two effects tend to cancel each other out.

3.7. Auxiliary heating and current drive

From a purely energetic point of view, all DEMO configurations proposed are ignited i.e., they produce enough heating power through fusion reactions to sustain the plasma in H-mode. However, for all configurations, a current drive power of 50 MW has been considered to be actuated by the electron cyclotron (EC) system, see also [58]. The assumption of a constant amount of installed (and used) heating and current drive (H&CD) power implies the same associated cost and complexity of the H&CD systems for all DEMO design points. Auxiliary CD has a positive impact on the device size since it relaxes a little the requirements on the solenoid by sustaining part of the plasma current (approximately 2.5 MA). In high A machines the central plasma temperature tends to be lower, and thus the current drive efficiency of the EC is reduced. At the same time the plasma current is lower too, thus the fraction of plasma current driven by the auxiliary system remains almost constant for all design points we found at ~10 %.

3.8. Central solenoid

The magnetic flux provided to the plasma is consumed for breakdown, ramp-up, sustainment of flat top as well as for shape and position control. This flux is predominantly provided by the CS. Its size is calculated by means of a look-up table, which requires as input the CS pre-magnetization flux, ψ_{preMag}, and the number of cycles to account for fatigue, as discussed below.

The flux consumed to generate the electric field during plasma breakdown, ψ_{BD}, has been set constant to 10 Wb – a value originating from studies of EU DEMO 2016.

The flux consumption during plasma ramp-up, ψ_{RU}, is calculated as.

$$\Psi_{RU} = \mu_0 R_0 I_p \left(\frac{l_{i,3}}{2} + C_{Ejima} \right)$$

where μ_0 is the magnetic permeability of vacuum. Unfortunately, neither the plasma internal inductance, $l_{i,3}$, nor the Ejima constant, c_{Ejim}, [101] are self-consistently calculated by PLASMOD. Thus, they have

been calculated with ASTRA for a single low-A DEMO case and set constant for all cases ($l_{i,3} = 0.65$ and $c_{Ejim} = 0.25$). This choice leads to somewhat optimistic values of ψ_{RU} in high-A cases, since low-A points tend to exhibit both a lower plasma inductance (because of their broader profiles) and a lower resistivity, and hence a lower c_{Ejim} (because of the higher plasma temperature).

For the calculation of the flux consumption during flat top, ψ_{FT}, the loop voltage, V_{loop}, is provided by PLASMOD, and it is consistent with the temperature and density profiles calculated by the transport model. Its value is multiplied with the flat-top duration, i.e., 2 h, to determine ψ_{FT}.

An accurate calculation of the flux consumed for plasma shaping and control during the entire pulse, ψ_{Sh}, would require detailed electromagnetic analyses on the entire plasma scenario (including ramps) in an iterative determination of the design point, a complexity that exceeds the scope of the present work. Hence ψ_{Sh} is calculated by a simple numerical fit, once more based on the data found for the EU DEMO 2016 case, namely:

$$\Psi_{Sh} = \frac{2}{3}(\Psi_{BD} + \Psi_{RU} + \Psi_{FT})$$

Incidentally, ψ_{Sh} is sometimes calculated by defining the so-called "external inductance" e.g., in the systems code PROCESS [102].

Since the CS is assumed to be operated from $-\psi_{preMag}$ to $+\psi_{preMag}$ the pre-magnetization flux requested to the CS is:

$$\Psi_{PreMag} = \frac{1}{2}(\Psi_{BD} + \Psi_{RU} + \Psi_{Sh} + \Psi_{FT})$$

Note that the simple tool we are employing does not allow for a detailed determination of ψ_{preMag}, and more accurate analyses are required for the final machine sizing. Values of the relevant flux terms are reported for DEMO and ITER in Table 6.

The central solenoid is a major driver of the tokamak size [105]. The definition of the magnetic flux provided by a solenoid, ψ_{preMag}, as a function of the radial thickness of the CS winding pack, t, shows the strong dependence on its average radius, R_T.

$$\Psi_{Premag} = \pi B_T R_T^2 \left[1 - \frac{t}{R_T} + \frac{t^2}{3R_T^2}\right]$$

The second relevant parameter is the magnetic field in the bore of the CS, B_T. It is, in practice, not a free parameter. In [43] it is found for a DEMO-relevant case and considering a non-graded conductor that the maximum flux for a given CS outer radius and a target fatigue lifetime of 30,000 plasma cycles is achieved for a peak field $B_T = \sim 14$ T. At higher B_T the required amount of steel notably reduces the engineering current density, J_{eng}, and thus a given flux requires a larger bore. Since both low-temperature superconductors (LTS) and HTS can be used at 14 T, it is reasonable for our purpose to fix B_T at 14 T.

The achievable current density defines the required thickness of the CS winding pack, t, and hence the radial size of the CS, $R_e = R_T + t/2$. While the current density in the superconductor is high (e.g., $J_{SC} = \sim 400$ A/mm^2 @ 14 T), J_{eng} is much lower due to the need to include steel, stabilizer, and insulation materials as well as coolant. The limit of the achievable J_{eng} is dominated by the required amount of steel and fatigue must be considered since the CS is a pulsed component. When the lifetime neutron fluence is prescribed, the number of pulses depends on the pulse length. The shorter the pulse length and the larger the number of pulses, the lower the allowable stress in the CS conductor jacket to prevent fatigue, requiring an increase of the steel cross-section and consequently a decrease of J_{eng}. The most important size driver of the CS size therefore is the allowable tensile hoop stress in the conductor steel, which depends on the type of steel and is related to the number of design cycles and the adopted crack growth model [106]. Since the size of the CS is so crucial, there is a high interest in maximizing the CS current density and to provide a maximum magnetic flux to the plasma from a compact CS:

- In [44] the regular replacement of the CS is considered to reduce its design life cycles.
- In [107] it is proposed to implement optimized CS conductors through the CS radius (graded conductor) considering the different levels of magnetic field using REBCO, Nb_3Sn and NbTi conductors with customized levels of steel. This approach has been adopted in a simplified way in the design of the TF coils of the DTT [108].
- In [109] the integration into the conductor of separate pipes for the coolant is considered to release the conductor jacket from the hydraulic function and the coolant pressure.
- We have recently initiated a review of the rules adopted in the structural integrity verification of the CS conductor jacket and have identified the potential to significantly reduce the conservatism in the partial safety factors, which will allow increasing the stress in the CS conductor. In addition, the choice of a probabilistic instead of a deterministic approach to verify the CS conductor jacket against non-ductile fracture might allow a further increase of the stress and hence of J_{eng}.

All four approaches achieve the desired increase of pre-magnetization flux but come at the cost of increased complexity and a lower level of maturity as compared to the conventional CS concept adopted e.g., in ITER [110] and JT60-SA [22]. For this design point study, we consider a free-standing conventional CS with non-graded cable-in-conduit conductor. Given the strong dependence of the machine size on the size of the CS and the available concepts to optimize its design, we provide DEMO design points considering *conservative* and *optimistic* CS conductor jacket design bases: in the conservative approach we consider 316LN as conductor jacket material and the conventional deterministic design rules to consider fatigue and non-ductile fracture. In the optimistic approach we consider the stronger JK2LB as jacket material, which has been developed for the ITER CS. Again, the conventional design rules are applied but not considering the usual safety factor of 2 on the number of cycles to reduce the high level of conservatism in these rules.

Table 6
Characteristic values driving the consumption of magnetic flux [Vs] in ITER and DEMO.

Pulse phase	ITER [103]	EU DEMO 2016 [104]	DEMO (A = 2.8)
A	3.1	3.1	2.8
R_0 [m]	6.2	8.9	7.95
I_p [MA]	15	19.07	20.8
c_{Ejim} / $l_{i,3}$	0.3/0.8	0.3/0.8	0.25/0.65
V_{loop} [mV]	75	30	~25
Flux consumption			
- Breakdown	10	10	10
- Ramp-up + shaping	220	399	326
- Flat top	30	216	180
- Total	**260**	**626**	**516**

3.9. TF coil

Based on the findings of [10] the "conventional" mechanical concept of the TF coils is considered here that has been developed for the NET TF coils [16] and was adopted in the ITER TF coil system [110]: the wedged TF coil inboard legs form a vault, which supports the unsupported radial EM forces through toroidal hoop stresses. For the TF coil structures the (ITER) high-strength steel is considered with yield strength >1000 MPa, [111]. The TF coil inboard legs are sized to allow the integration of the winding pack and the structures required to withstand the EM forces, see appendix A. In the sizing of the winding pack, we also consider electrical insulation. We recognize that the insulator is not needed during normal operation when the TF coils are operated at constant current and, due to superconductivity, at zero voltage. However, in an event when

superconductivity is locally lost (→ quench [112]), a fast discharge of the coils should be foreseen to avoid unrecoverable damage due to the generated heat. The magnetic energy stored in small coils (such as those of magnetic resonance imaging) can be dissipated in the coils themselves. However, the several GJ of stored magnetic energy in tokamaks [10] requires external dump resistors for the discharge during which a high voltage occurs on the coils requiring an insulator.

The shape of the TF coils should consider the large EM pressure due to their magnetization. Energized TF coils arranged in a toroidal configuration experience only membrane forces when a *bending-free shape* is chosen [113]. Taking advantage of this D-shape becomes increasingly important in large machines or in case of a high magnetic field when large EM forces occur. Since DEMO is a very large machine, we consider TF coils with a bending-free D-shape. We recognize that the less elongated shape of a plasma with high aspect ratio does not make good use of the valuable volume inside the more elongated TF coils with bending-free shape, see [10].

3.10. Vacuum vessel and breeding blanket

In contrast to most existing fusion machines that generate a small or modest number of neutrons, a substantial neutron shield is required in a fusion power plant. This is provided by the vacuum vessel (VV) and the blanket, which limit the heat load on the TF coils, the radiation damage to its electrical insulators and superconductors, and the activation of the structures outside the VV. Due to the space constraints on the inboard side of tokamaks with low A, the neutron shielding structures implemented in related power plant studies are generally insufficient, see [60] and Table 7. Replacing the steel/water mixture implemented in ITER with materials with better n-shielding performance would allow reducing the thickness of the n-shield. E.g., the use of tungsten-carbide or borated tungsten may allow a reduction of the n-shield by 100–200 mm [114] at the price though of higher VV cost. Increasing the tolerance of superconductors to heat loads is the alternative approach to allow a reduction of the n-shielding structures. It is hoped that high-temperature superconductors (HTS) could be operated at higher levels of neutron heating [85,9]. This assumption is however challenged by the low allowable neutron fluence of the epoxy insulator [115], see also previous section. The use of copper instead of superconductors in the TF coils as considered e.g., in [72,85,116], and [52] is unfeasible for a power plant due to the high Joule losses (>300 MW in ARIES-ST [72], ~10 GW estimated for a DEMO-size device) and would also require active cooling of the copper conductors [72,116]. It is for this reason that superconductivity has been seen since the early days as enabling technology for the realization of fusion energy [117] and the associated requirement for sufficient n-shielding is a caveat that cannot be avoided.

Given the tritium breeding rate of state-of-the-art BB concepts [119, 120] a large radial build of the BB of ~800 mm is required on the inboard side to achieve a sufficiently high tritium breeding ratio (TBR) [3]. Many reactor studies therefore omit the BB compromising the often-made promise of tritium self-sufficiency [72,83]. In [9] it is proposed instead replacing the thick BB on the inboard side with a more compact neutron reflector (Pb being the most effective material choice) suggesting that sufficient T-breeding could then be achieved by the BB on the outboard. We repeated this assessment for DEMO but found much lower n-reflections. This is likely due to our use of the MCNP Monte Carlo computer code with a 3D geometry and modern nuclear data assuming its continuous energy representation instead of a simplified 1D cylindrical geometry and a deterministic neutron transport code utilizing 30 neutron energy groups as nuclear data. We found the probability of the backscattering from Pb for 1 MeV neutrons is ~15 % but these make up less than 8 % of the neutrons in the BB first wall and are significantly less effective breeding tritium through an interaction with lithium. The more effective and also more abundant 14 MeV neutrons are however reflected with a much lower probability of only ~0.2 %, which is negligible in this context. Therefore, neutron reflection from the inboard blankets cannot increase the tritium breeding in the outboard blankets by more than a few percent. We therefore conclude that without integrating a breeding blanket on the inboard side, that makes up approximately 30-40 % of the total wall surface [121], tritium self-sufficiency is not achievable unless more efficient BB concepts were available e.g., based on (fission) n-multiplier materials such as U238 as considered in [27].

Consequently, the thickness of the VV and the BB is constant in all design points: 1.37 m [118]. The radial build includes in addition: (i) a distance between the plasma and the wall of 150 mm, and (ii) a gap between TF coil and VV of ~100 mm to integrate the thermal shield. Hence the distance considered between plasma and TF coil on the inboard side is 1.6 m.

We note that a significant reduction of the inboard BB (by a few hundred mm) would be possible if the BB would achieve a slightly higher and less marginal tritium production rate. In devices with a low aspect ratio, where the wall surface fraction of the inboard side is small, this effect is stronger since. The reduced n-shielding performance of a slimmer BB could be compensated by a minor increase of the VV thickness (by few tens of mm).

Table 7
Aspect ratio, TF conductor type, and thicknesses of the neutron shield, t_{shield}, and of the BB, t_{BB}, in selected power plant studies based on spherical tokamaks and comparison to ITER and power plant studies with higher aspect ratio machines

	A	TF conductor	$t_{shield} + t_{BB}$
ARIES-ST [72]	1.6	Cu alloy	0.20+0.0 = 0.20 m
UK-ST135 [78]	1.8	HTS	0.35+0.0 = 0.35 m
ARC [77]	2.9	HTS	0.59+0.2 = 0.79 m
ITER [26]	3.1	LTS	0.73+0.0 = 0.73 m
ITER 1996 [27]	2.7	LTS	1.3 m
EU DEMO [118]	3.1	LTS	0.60+0.77 = 1.37 m

4. Results of the design exploration

4.1. Identified size of DEMO

Design points of DEMO with minimum size were identified for aspect ratios in the range A = 2.2 – 5.0 considering the performance requirements and input parameters and requirements described above, see Fig. 2. It is notable that the magnetic field, B_0, is linearly dependent on the aspect ratio, A. An important reason is the safety factor, q, which is naturally higher in a plasma with low aspect ratio (since $q \sim B/(AI_p)$, and also because of the higher elongation). Hence the field can be lowered in case of lower A. This relationship, $A \sim B_0$, was also recognized in studies of the ITER design point [90]. The correlation of high magnetic field with high aspect ratio is also reflected by the choices made in the reactor studies shown in Fig. 1.

For $A < \sim 2.6$ the space available for the CS is tight and solutions are found only when the major radius is increased significantly, which leads to unattractively large machines. For aspect ratios $A > \sim 3.3$ no further appreciable reduction of the tokamak size is possible and for $A > 4$ the tokamak size even increases due to the large space claim of the TF coils. For large machines such as DEMO the choice of a high aspect ratio is, however, even more restricted. At high A the associated high magnetic field requires excessively large structures to resist the EM loads acting on the TF coils, see [10] and [11]. Even at a conventional aspect ratio, $A = 3.1$, no practical manufacturing route could be identified for DEMO [5]. We consider DEMO TF coils as realizable up to an aspect ratio of approximately 3.0, which corresponds to a magnetic field on the plasma axis of 5.4 T.

To reasonably limit the size of EU DEMO and to ensure the feasibility of its TF coils the aspect ratio must be chosen within the range $A = \sim 2.6$ - ~ 3.0. Within this range the tokamak size reduces moderately towards higher aspect ratios while the magnetic field and the heat loads on the divertor increase, see next sub-section.

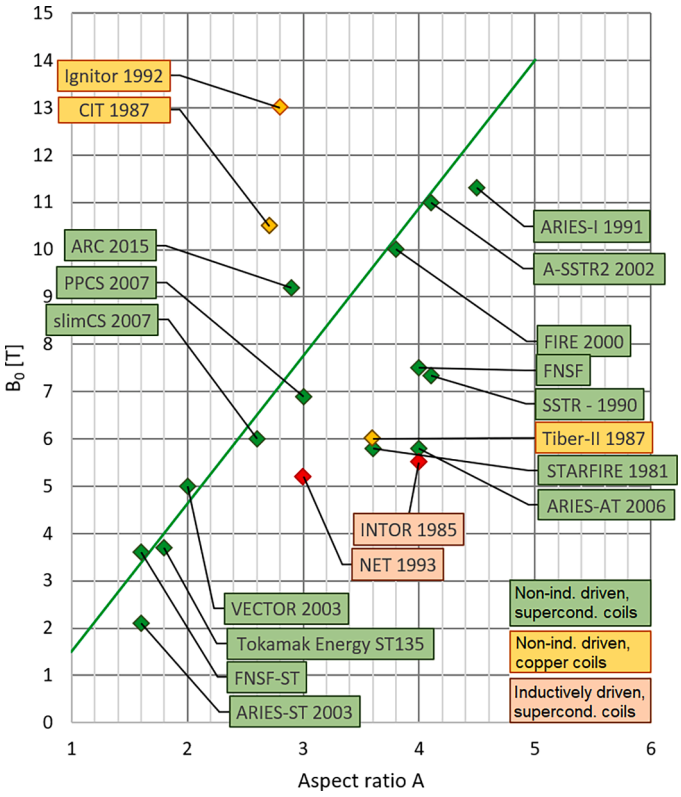

Fig. 1. Relation of aspect ratio and magnetic field in selected tokamak reactor studies and trendline indicating an approximate relation of magnetic field with aspect ratio.

4.2. Divertor heat loads

According to the broadly employed Eich scaling [122,123], the heat load channel width in the scrape-off-layer, λ_q, scales unfavourably with the field strength, B_0, and very weakly with the major radius, R.

$$\lambda_q = 0.73 B_0^{-0.78} q_{95}^{1.2} R^{0.1}$$

As previously discussed, due to the presence of core radiation, the assumption has been made that the power crossing the separatrix for the design points considered is proportional to P_{LH}, following the widely employed Martin scaling:

$$P_{LH} = 0.049 n^{0.72} B_0^{0.8} A_{pl}^{0.94}$$

where A_{pl} is the plasma surface. The plasma density, n, as previously mentioned, has been assumed proportional to the Greenwald density limit, n_{GW} [124]:

$$n \propto n_{GW} = \frac{I_p}{\pi a^2}$$

where I_p is the plasma current and a is the minor plasma radius.

The heat flux on the divertor in attached condition, $Q_{target,attached}$, is then proportional to the power crossing the separatrix divided by the wetted area, which in turns depends on λ_q:

$$Q_{target,attached} \propto \frac{P_{sep}}{2\pi R \lambda_q}$$

Assuming a constant plasma shape (q_{95}, elongation and triangularity), Siccinio et al. [125] show that:

$$Q_{target,attached} \propto B_0^{\ 2.52} R^{0.16}$$

This last relation indicates that generally speaking, *a high-field device is expected to be more challenging in terms of power exhaust.* We recognize that no fusion power reactor is foreseen to operate in attached divertor condition and that a reduction of $Q_{target,attached}$ must eventually be considered due to the detachment. However, the divertor heat flux under attachment is a representative figure of merit and provides a good indication of the challenge of the power exhaust problem. The strong dependency of the divertor heat loads to the magnetic field strength is discussed also in [11]. Incidentally, we note that this supports the conception that an increase of the field strength increases the power density of the device.

4.3. VV loads during TF coil fast discharge

As discussed above, in large tokamaks with high magnetic energy a quench detection system is implemented to trigger a fast discharge via dump resistors. The electrical resistivity of the dump resistor together with the coil inductance defines the characteristic time constant, $\tau_{discharge}$, of the exponential current decay during the discharge. When operating at higher magnetic fields the discharge of the TF coils must be slowed down to $\tau_{discharge,TFC\text{-}Voltage}$ to not exceed the imposed limit of the TF coil voltage, which has been considered for DEMO as ~10 kV terminal to terminal, see Table 8. Consequently, the amount of Cu-stabilizer in the conductor must be adjusted to prevent damage during the quench. This leads to a further reduction of the engineering current density and hence an increased space claim of the TF coil.

We also assessed the EM forces acting on the VV as a consequence of the TF coil fast discharge for the DEMO design points considered in [10]. During the fast discharge a poloidal eddy current is induced in the VV. It generates, in combination with the decaying but still strong toroidal magnetic field, considerable Lorentz forces on the VV structure. The EM pressure on the VV shells acts outwards, away from the plasma, and is particularly strong on the inboard side. In machines larger than ITER with high magnetic energy [10], the TF coil discharge must be sufficiently slow to prevent buckling of the VV inboard wall [126]. Consequently, the VV was reinforced in DEMO using higher-strength steel and implementing toroidal ribs [127]. A study, coupling an electromagnetic with a structural finite element model, determined for DEMO the shortest possible discharge of the TF coils to avoid buckling of the VV, expressed by $\tau_{discharge,VV}$. It is calculated such that the pressure load on the VV inboard wall would cause a toroidal compressive stress of 150 MPa, which is postulated to be the buckling limit. In the analysis the EM pressure acting on the VV inboard wall of ~2 MPa is further increased by an equivalent pressure of ~0.4 MPa due to the ferromagnetic force acting on the BB. Note that $\tau_{discharge,VV}$ should be increased at least by a factor of 1.5 to ensure a reasonable margin against buckling. The study finds a strong dependency of $\tau_{discharge,VV}$ on the magnetic field strength, see Table 8. However, the driver for the definition of the time constant of the fast discharge is in all cases the requirement to limit the TF coil voltage. In the case of a higher magnetic field more substantial provisions are needed to not exceed this limit.

Table 8
Minimum TF coil discharge time constants for DEMO design points with different aspect ratios to limit (i) the coil voltage ($\tau_{discharge,TFC\text{-}Voltage}$), and (ii) the EM pressure acting on the VV ($\tau_{discharge,min,VV}$).

Design point	A=2.6	A=3.1	A=3.3	A=4.5
R	7.5 m	8.9 m	6.5 m	7.4 m
B_0	4.0 T	5.8 T	6.5 T	11.7 T
$R_{VV,inb}$	3.1 m	4.5 m	3.1 m	4.3 m
Max. coil voltage	9 kV	11 kV	8 kV	9 kV
$\tau_{discharge,VV}$	3.9 s	10.1 s	9.5 s	18.1 s
$\tau_{discharge,\ TFC\text{-}Voltage}$	16 s	28 s	18 s	38 s
$\tau_{discharge}$	16 s	28 s	18 s	38 s

4.4. In-vessel remote maintenance

Access to the in-vessel components and their cooling pipes is a critical aspect to be considered in the basic design of EU DEMO. Main obstacle are the magnet coils, which enclose the VV in a cage-like structure limiting the size of the VV ports. Demountable coils as proposed in several American studies e.g., [72], are not considered in DEMO because dismantling and reinstallation of large parts of the magnet system is impractical. We assume here the remote handling (RH) concepts described in [118] i.e., slightly inclined lower ports to replace the divertor and vertical upper ports to replace the blanket. Since the removal of the large BB segments is particularly challenging, [1], we focused here on the accessibility of these.

The critical toroidal size of the upper VV port is limited by the space in-between adjacent TF coils. Also, the size of the blankets, which must pass through the port, is relevant. Their proportionality does not significantly change with the aspect ratio. Although the TF coils of a DEMO tokamak with higher magnetic field (and higher aspect ratio) are significantly more massive, their toroidal dimension is similar to that of TF coils in a DEMO tokamak with lower field since they are arranged on the inboard side to form a vault. In DEMO tokamaks with 16 TF coils and with different aspect ratios the space available to integrate cooling pipes on the accessible backside of the blanket segments as well as for the blanket removal kinematics through the upper port is similarly limited with respect to the size of the blankets, see Fig. 3. We noted instead that the accessibility reduces significantly for larger numbers of TF coils. We conclude that the impact of the aspect ratio on the challenge of in-vessel maintenance is minor.

4.5. Capital cost

In the context of this article the impact of aspect ratio and magnetic field strength on the cost of EU DEMO is of interest. For this purpose, we estimated the main cost factors of DEMO and identified scaling factors, see Table 9. The cost of many tokamak components scales with the tokamak size and thus can be expected to reduce moderately when the aspect ratio is increased up to $A = \sim 3.5$, see Fig. 2. At the same time the cost of the TF coils increases notably due to the higher magnetic field [11]. We recognize the significant uncertainty associated with cost figures.

We conclude that within the range of realizable aspect ratio values, $2.6 < A < 3.0$, the cost impact of the magnetic field (and A) is minor also due to the high cost of the plant systems that is not much affected by the size of the tokamak, see Fig. 4.

5. Summary and conclusions

In the design definition of a tokamak the goal has traditionally been to find the most compact configuration of the machine components and of the plasma for a given set of performance parameters. We performed a system code study to size the EU DEMO tokamak. Its size depends on the performance requirements for fusion power and pulse length, and we find that the DEMO major radius, R_0, must be larger than 8 m for the machine to provide 2 GW of fusion power in pulses of at least two hours. The reduction of the pulse length from 2 h to 1 h would allow reducing the major radius by ~0.4 m. The additional reduction of the fusion power requirement from 2000 MW to 760 MW would allow a further reduction of the major radius by another ~0.4m.

Table 9
Assumed scaling of main cost items.

	Scaling
Magnet system	$A_{pl} \cdot B_0^2$
VV and IVCs	A_{pl}
RH tools and active maintenance facility	A_{pl}
Most remaining plant systems + site	1.0

The approach to drive the plasma current - inductively or non-inductively - has been reviewed because of its major impact on the machine size. The lack of a reliable physics basis with a bootstrap current fraction significantly exceeding 50 % of I_p, and the large power consumption of auxiliary current drive systems, require that next step tokamak devices defined today must be pulsed relying on inductive current drive, unless higher risk is accepted.

Three main factors limit the size reduction of the DEMO tokamak, namely (i) the required size of the plasma to reach burning plasma conditions in its core, (ii) the space required for a large central solenoid to drive the plasma current inductively, and (iii) the space required on the inboard side to breed tritium and to protect the superconducting coils from n-irradiation, which causes the plasma to be shifted towards the lower field region on the outboard. We found the T-breeding and n-shielding structures under-dimensioned in most reactor studies although the required thickness of VV and BB is largely independent of the reactor configuration.

The aspect ratio, A, is the only free major geometric parameter, its choice however affects important machine parameters such as the plasma current, the magnetic field, the power exhaust conditions, and also the major radius. We therefore determined minimum-size DEMO design points scanning the plasma aspect ratio and made the following major findings:

- When scanning for the smallest machine size, B_0 is roughly linearly dependent on A.
- At lower aspect ratio the plasma performs equally well in a lower magnetic field and has a higher natural elongation. Hence, in principle, A should be minimized.
- Increasing aspect ratio and magnetic field strength allows reducing the tokamak size up to $A \sim 4$, which is associated to $B_0 \sim 9\ T$. Above $A \sim 3.1$ the possible machine size reduction is however moderate. In machines with $A > 4$ and $B_0 > 9\ T$ rather than the plasma or the CS it is the TF coil system designed to sustain the very high EM loads that dominates the size of the tokamak.

A lower limit to A is given by the space required on the inboard side to integrate CS, BB, VV and the TF coils. We found this limit for DEMO to be approximately $A_{min,DEMO} = \sim 2.6$. An upper limit to A is given by the divertor heat loads and the design of the magnets and their structures. For DEMO we found this limit to be approximately $A_{max,DEMO} = \sim 3.0$ noting that the divertor heat loads may eventually impose a lower limit. Within this range the magnetic field on the TF coil conductor is lower than ~12.5 T. Then the potential to reduce the size of the TF coil winding pack by replacing Nb_3Sn with HTS is minor. We also found the CS rather than the TF coils to be the main driver of the inboard radial build and hence of the machine size. Again, the consideration of HTS in the CS does not allow reducing its size significantly, as it is dominated by structural material limits.

The aspect ratio of DEMO should be chosen within the range $A = \sim 2.6$ - ~ 3.0 trading-off the machine compactness against magnet design and divertor heat loads.

The greatest potential regarding the reduction of the DEMO size lies in the following points:

- The development of plasma scenarios with improved confinement.
- The development of plasma regimes of operation with higher bootstrap current fraction approaching steady-state scenarios. (We find a bootstrap current fraction of $f_{BS} = \sim 38$ %. Our literature research suggests that $f_{BS} > 40\text{-}50$ % cannot be considered as realistic.)
- Linked to the previous point, the development of a robust and reliable RWM control concept would allow operating with a higher β_N value and to reduce the plasma current.
- An advanced concept of the CS, providing more magnetic flux within the same space. This would require a structural material with a

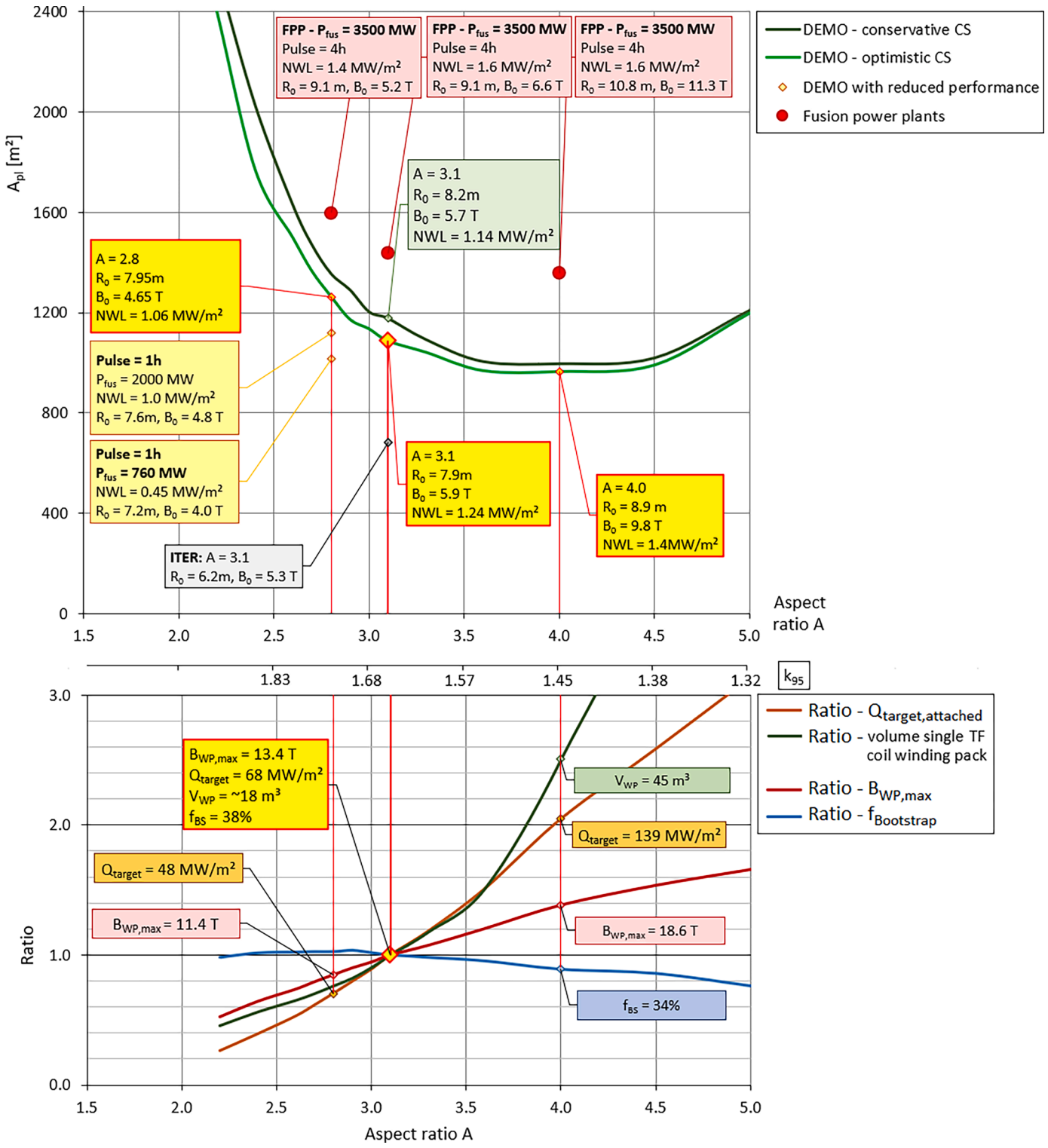

Fig. 2. Top: Minimum DEMO size represented by the plasma surface area, A_{pl}, depending on the aspect ratio, A, achieving the performance requirements, namely $P_{fus} = 2000$ MW and pulse length 2h, for conservative or optimistic sizing rules of the CS. Above the curves design points exist of reactors with greater performance, below the curves with reduced performance. Also shown: indication of design points of fusion power plant with postulated performances. Bottom: dependence of characteristics i.e., heat load on divertor targets in attached condition, volume of TF winding pack, maximum field on TF conductor and bootstrap current fraction, relative to a DEMO design point with $A = 3.1$

higher cyclic tensile strength as compared to the cryogenic steels we have considered so far, or fatigue design criteria with reduced conservatism.

- Neutron shielding materials with higher neutron attenuation as compared to steel e.g., tungsten carbide or borated tungsten.
- A BB achieving a tritium breeding rate high enough to require its installation on the outboard side only. The BB on the inboard side could then be replaced by a significantly more compact n-shielding blanket.

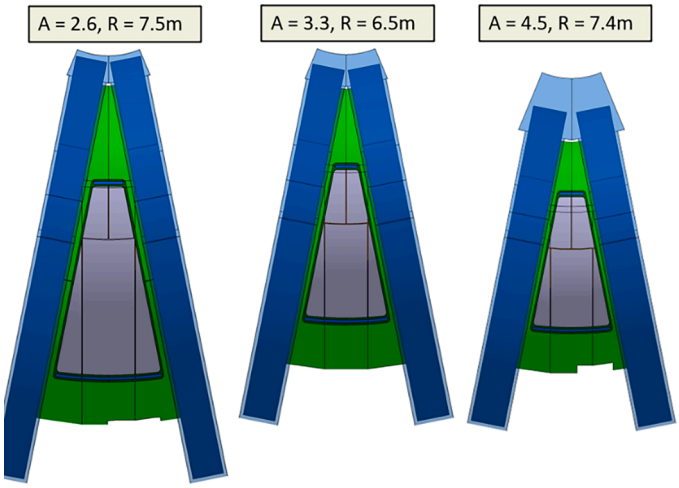

Fig. 3. Vertical view from the top on a single upper VV port (green) in-between two TF coils (blue). The accessible parts of the blanket backsides (grey) scale approximately with the upper port size in the three displayed tokamak configurations with different aspect ratios. Note: absolute size of these tokamak machines is more compact as compared to what is shown in Fig. 2. The geometric dependencies are relevant, nonetheless.

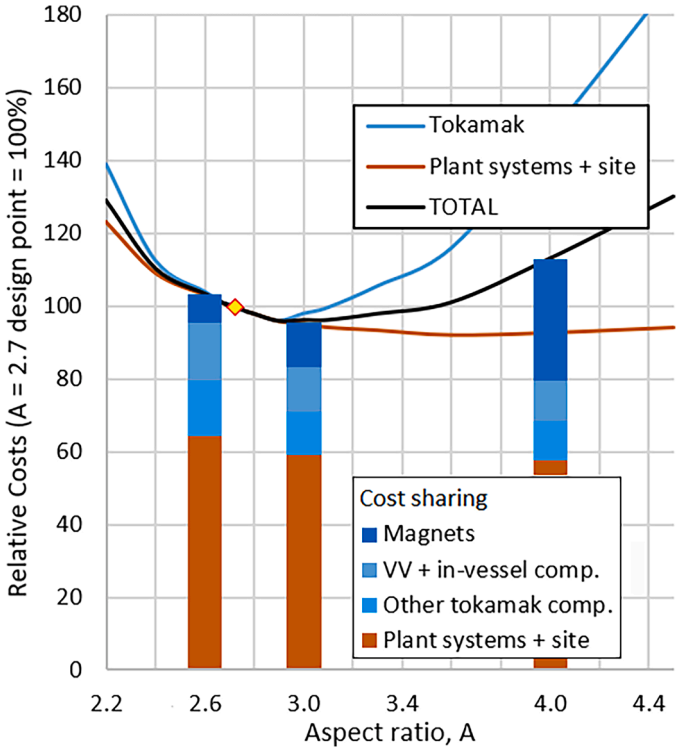

Fig. 4. Relative cost of EU DEMO for different values of A compared to $A = 2.7$ and cost sharing at three selected values of A.

For maximum impact and to accelerate fusion deployment, research, development, and qualification should concentrate on the points above.

CRediT authorship contribution statement

C. Bachmann: Writing – original draft, Validation, Supervision, Methodology, Investigation, Conceptualization. **M. Siccinio:** Writing – original draft, Validation, Methodology, Conceptualization. **A. Ciula:** Writing – review & editing, Formal analysis. **P. Fanelli:** Supervision. **G. Federici:** Validation, Supervision, Methodology. **L. Giannini:** Writing – review & editing, Formal analysis, Conceptualization. **C. Luongo:** Writing – review & editing, Supervision, Methodology. **P. Pereslavtsev:** Writing – review & editing, Methodology, Formal analysis. **X. Sarasola:** Writing – review & editing, Visualization, Methodology, Formal analysis. **T. Steinbacher:** Visualization, Methodology, Conceptualization. **H. Zohm:** Validation, Supervision, Methodology.

Declaration of competing interest

The authors declare that they have no known competing financial interests or personal relationships that could have appeared to influence the work reported in this paper.

Data availability

No data was used for the research described in the article.

Acknowledgments

This work has been carried out within the framework of the EUROfusion Consortium, funded by the European Union via the Euratom Research and Training Programme (Grant Agreement No 101052200 — EUROfusion). Views and opinions expressed are however those of the author(s) only and do not necessarily reflect those of the European Union or the European Commission. Neither the European Union nor the European Commission can be held responsible for them.

The authors wish to thank Günter Janeschitz, Carlo Damiani (Fusion 4 Energy), Christian Day (KIT), Thomas Franke, Curt Gliss, Ivo Moscato and Sergio Ciattaglia (all with EUROfusion) for the constructive discussions regarding the cost estimates, Alfredo Portone (F4E) for the consultations regarding the functions of the central solenoid, and Emiliano Fable for the support with PLASMOD.

Appendix A: Sizing formulae of TF coils

This appendix provides the calculation basis used in our system code study to size the TF coils on the inboard side of EU DEMO depending on the plasma major radius, R, the plasma minor radius, a, the magnetic field on the plasma axis, B_0, the number of TF coils, n_{TF}, and the distance between plasma and TF coil winding pack, w_p.

The total electrical current in a single TF coil is calculated as:

$$I_{TF} = 2\pi \frac{B_0 \cdot R_0}{n_{TF} \cdot \mu_0},$$

where μ_0 is the magnetic permeability in vacuum.

The radial location of the TF coil winding pack (VV side) is:

$$R_i = R_0 - a - w_p$$

The maximum field on a TF conductor, B_{max}, is calculated applying a factor of 1.08 to consider the TF coil winding packs being arranged on the inboard side in the shape of a polygon rather than a cylinder:

$$B_{max} = 1.08 \cdot \frac{B_0 \cdot R_0}{R_i}$$

The required cross-section of the TF coil winding pack, A_{WP}, is the fraction of I_{TF} by the engineering current density, J_{eng}. The latter depends on B_{max} and is estimated from relevant winding pack designs developed for different design points following the procedure described in [128] considering either LTS or HTS:

- $J_{eng,LTS}\ [A/mm^2] = 47.8 - 1.43 \cdot B_{max}\ [T],\ B_{max} < 15\ T,$
- $J_{eng,HTS}\ [A/mm^2] = 55.8 - 1.92 \cdot B_{max}\ [T],\ B_{max} > 15\ T.$

Note: The values considered for J_{eng} are applicable to DEMO-size magnet coils only.

The radial size of the winding pack, $t_{inb,WP}$, is calculated assuming a trapezoidal cross-section allowing for a 100 mm thick steel case on both lateral sides. The radius of the winding pack centerline on the inboard is calculated as $R_{TF,inb} = R_i - 0.5 \cdot t_{inb,WP}$. The radius of the winding pack centerline on the outboard is defined to limit the TF ripple on the plasma to 0.6 % according to the approach used in the PROCESS code [102]. The inner part of the TF coil inboard case i.e., the "nose", is sized to withstand the EM forces that occur due to the magnetization of the TF coils. The vertical separation force and the radial force per meter vertical length in the inboard leg of a single TF coil, see also [10], are calculated as:

$$F_{sep,TF,inb} = \frac{R_0 \cdot B_0 \cdot I_{TF}}{4} \cdot \left(ln\ R_{TF,outb} - lnR_{TF,inb}\right)$$

$$F_{rad,TF,inb}/m = \frac{B_{max} \cdot I_{TF}}{2}$$

The toroidal compressive force given the wedged support concept of the TF coils [129] follows as:

$$F_{tor,TF,inb} = \frac{-F_{rad,TF,inb}}{2 \cdot \sin(\pi/n_{TF})}$$

The TF coil nose is sized considering a v. Mises stress limit of 660 MPa for the radial and toroidal forces, $F_{sep,TF,inb}$ and $F_{rad,TF,inb}/m$, deducting the part carried by the winding pack. The latter is calculated assuming an average vertical tensile and toroidal compressive stress in the winding pack of 65 MPa.

References

[1] A.J. Donné, Roadmap towards fusion electricity, J. Fusion Energy 38.5 (2019) 503–505.
[2] G. Federici, et al., Overview of EU DEMO design and R&D activities, Fusion Eng. Des. 89 (2014) 882–889.
[3] G. Federici, et al., Overview of the design approach and prioritization of R&D activitiestowards an EU DEMO, Fusion Eng. Des. 109–111 (2016) 1464–1474.
[4] R. Wenninger, et al., The physics and technology basis entering European system code studies for DEMO, Nucl. Fusion 57 (2017) 016011.
[5] V. Corato, et al., The DEMO magnet system–Status and future challenges, Fusion Eng. Des. 174 (2022) 112971.
[6] W.H. Fietz, et al., High temperature superconductors for the ITER magnet system and beyond, Fusion Eng. Des. 75 (2005) 105–109.
[7] AE. Costley, Towards a compact spherical tokamak fusion pilot plant, Phil. Trans. R. Soc. A 377 (2019) 20170439.
[8] Hartwig, Z. "The SPARC toroidal field model coil." Invited Oral Presentation at MT-27 (2021).
[9] B.G. Hong, Conceptual study of a superconducting ST reactor with a self-consistent system analysis code, Nucl. Fusion 51 (2011) 113013.
[10] C. Bachmann, et al., Influence of a high magnetic field to the design of EU DEMO, Fusion Eng. Des. 197 (2023) 114050.
[11] G. Federici, et al., Relationship between magnetic field and tokamak size – A system engineering perspective and implications to fusion development, Nucl. Fusion 64 (2024) 036025.
[12] D.L. Jassby, SMARTOR: A Small-Aspect-Ratio Torus For Demonstrating Thermonuclear Ignition. No. PPPL-1371, Princeton Univ., NJ (USA). Plasma Physics Lab, 1977.
[13] YK M. Peng, D.J. Strickler, Features of spherical torus plasmas, Nucl. Fusion 26.6 (1986) 769.
[14] Huguet M. et al, Design, manufacture and assembly of the JET machine, philosophical transactions of the royal society of London. Series A, mathematical and physical sciences, Jun. 29, 1987, Vol. 322, No. 1563, the JET project and the prospects for controlled nuclear fusion (Jun. 29, 1987), pp. 31–46.
[15] E. Bertolini, JET with a pumped divertor: design, construction, commissioning and first operation, Fusion Eng. Des. 30 (1995) 53–66.
[16] The NET device - Introduction and executive summary, Fus. Eng. Des. 21 (1993) 3–15.
[17] INTERNATIONAL ATOMIC ENERGY AGENCY, ITER Conceptual Design Report, ITER Documentation Series, IAEA, Vienna, 1991.
[18] R. Albanese, WPDTT2 Team, DTT: a divertor tokamak test facility for the study of the power exhaust issues in view of DEMO, Nucl. Fusion 57.1 (2016) 016010.
[19] A.W. Morris, MAST: results and upgrade activities, IEEE Trans. Plasma Sci. 40 (2012) 682.
[20] J.E. Menard, et al., Overview of NSTX Upgrade initial results and modelling highlights, Nucl. Fusion 57.10 (2017) 102006.
[21] P.P. Khvostenko, Current status of tokamak T-15MD, Fus. Eng. Des. 164 (2021) 112211.
[22] H. Shirai, P. Barabaschi, Y. Kamada, and the JT60SA Team, Recent progress of the JT-60SA project, Nucl. Fusion 57 (2017). Art. no. 102002.
[23] J.L. Luxon, A design retrospective of the DIII-D tokamak, Nucl. Fusion 42 (2002) 614.
[24] G. Federici, et al., DEMO design activity in Europe: Progress and updates, Fusion Eng. Des. 136 (2018) 729–741.
[25] Ge Zhuang, et al., Progress of the CFETR design, Nucl. Fusion 59.11 (2019) 112010.
[26] R. Aymar, The ITER design, Plasma Phys. Control. Fusion 44 (2002) 519.
[27] P.H. Rebut, Reflections on Fusion Future, European Commission, 1996.
[28] Y. Kusama, M. Yamamoto, JFT-2M Group, JFT-2M program, Fusion Sci. Technol. 49.2 (2006) 89–95.
[29] N. Hosogane, Development and operational experiences of the JT-60U tokamak and power supplies, Fusion Sci. Technol. 42 (2002).
[30] P. Rodriguez-Fernandez, et al., Overview of the SPARC physics basis towards the exploration of burning-plasma regimes in high-field, compact tokamaks, Nucl. Fusion 62.4 (2022) 042003.
[31] K. Lackner, Recent results from divertor operation in ASDEX upgrade, Plasma Phys. Control. Fusion 36 (1994) B79.
[32] S. Coda for the TCV Team, Overview of recent and current research on the TCV tokamak, Nucl. Fusion 53 (2013) 104011.

[33] G.S. Lee, The design of the KSTAR tokamak, Fusion Eng. Des. 46 (1999) 405–411.
[34] S. Wu, An overview of the EAST project, Fusion Eng. Des. 82 (2007) 463–471.
[35] J. Bucalossi, et al., Feasibility study of an actively cooled tungsten divertor in Tore Supra for ITER technology testing, Fusion Eng. Des. 86 (2011) 684.
[36] D. Maisonnier, et al., Power plant conceptual studies in Europe, Nucl. Fusion 47.11 (2007) 1524.
[37] H. Zohm, et al., On the physics guidelines for a tokamak DEMO, Nucl. Fusion 53 (2013) 073019.
[38] M. Siccinio, et al., Development of the plasma scenario for EU-DEMO: status and plans, Fusion Eng. Des. 176 (2022) 113047.
[39] Uckan, N. A. "ITER physics design guidelines: 1989." (1990).
[40] R. Wenninger, et al., The DEMO wall load challenge, Nucl. Fusion 57.4 (2017) 046002.
[41] Y.R. Martin, T. Takizuka, Power requirement for accessing the H-mode in ITER, J. Phys. Conf. Ser. 123 (1) (2008) 012033.
[42] ITPA, H, Roles of aspect ratio, absolute B and effective Z of the H-mode power threshold in tokamaks of the ITPA database, Plasma Phys. Control Fusion. 46.5A (2004) A227–A233.
[43] X. Sarasola, et al., Parametric studies of the EU DEMO central solenoid, IEEE Trans. Appl. Supercond. 33.5 (2023) 1–5.
[44] D.A. Ehst, et al., Tokamak Burn Cycle Study: A Data Base for Comparing Long Pulse and Steady-State Power Reactors, Rep. ANL/FPP/TM-178, Argonne National Lab., Illinois, 1983.
[45] M. Yoshikawa, An overview of the J-60 project, Fusion Eng. Des. 5 (1987) 3–8.
[46] C.E. Kessel, Bootstrap current in a tokamak, Nucl. Fusion 34 (1994) 1221.
[47] R.J. Bickerton, J.W. Connor, J.B. Taylor, Nature (London) Physics, Science 229.1 (1971) 10.
[48] M.C. Zarnstorff, et al., Bootstrap current in TFTR, Phys. Rev. Lett. 60.13 (1988) 1306.
[49] F.L. Hinton, R.D. Hazeltine, Theory of plasma transport in toroidal confinement systems, Rev. Mod. Phys. 48.2 (1976) 239.
[50] X.Z. Gong, et al., EAST steady-state long pulse H-mode with core-edge integration for CFETR, Nucl. Fusion 62.7 (2022) 076009.
[51] J.E. Menard, et al., Overview of the physics and engineering design of NSTX upgrade, Nucl. Fusion 52.8 (2012) 083015.
[52] G.M. Voss, A. Bond, J.B. Hicks, H.R. Wilson, Development of the ST power plant, Fusion Eng. Des. 63 (2002) 65–71.
[53] H.R. Wilson, et al., Integrated plasma physics modelling for the Culham steady state spherical tokamak fusion power plant, Nucl. Fusion 44.8 (2004) 917.
[54] K. Hanada, et al., Power balance investigation in steady-state LHCD discharges on TRIAM-1M, Fusion Eng. Des. 81.19 (2006) 2257–2265.
[55] B. Saoutic, M. Chatelier, C. De Michelis, Tore supra: toward steady state in a superconducting tokamak, Fusion Sci. Technol. 56:3 (2009) 1079–1091.
[56] P.K. Sharma, et al., Current drive experiments in SST1 tokamak with lower hybrid waves, Nucl. Fusion 62.5 (2022) 056020.
[57] A. Bock, et al., Non-inductive improved H-mode operation at ASDEX Upgrade, Nucl. Fusion 57.12 (2017) 126041.
[58] M.Q Tran, Status and future development of heating and current drive for the EU DEMO, Fusion Eng. Des (2022).
[59] Y. Ogawa, et al., A low wall-loading DEMO reactor design with high priority for early and reliable realization of a tokamak fusion reactor over the cost performance, J. Fusion Energy 14.4 (1995) 353–359.
[60] D.J. Segal, Nucl. Fusion 61 (2021) 045001 (40pp).
[61] D.J. Campbell, et al., Innovations in technology and science R&D for ITER, J. Fusion Energy 38 (2019) 11–71.
[62] S. Ding, A.M. Garofalo, Progress in the development and understanding of a high poloidal-beta tokamak operating scenario for an attractive fusion pilot plant, Rev. Mod. Plasma Phys. 7.1 (2022) 4.
[63] H. Zohm, et al., A stepladder approach to a tokamak fusion power plant, Nucl. Fusion 57.8 (2017) 086002.
[64] W.M. Stacey Jr, et al., INTOR—a first-generation tokamak experimental reactor, Nucl. Eng. Des. 63.2 (1981) 171–187.
[65] A.J. Creely, et al., Overview of the SPARC tokamak, J. Plasma Phys. 86.5 (2020) 865860502.
[66] K. Tobita, et al., Conceptual design of Japan's fusion DEMO reactor (JADEMO) and superconducting coil issues, J. Phys. Conf. Ser. 1293 (1) (2019) 012078.
[67] Ignat, D. W. "Recent progress on the Compact Ignition Tokamak (CIT)." (1987).
[68] C.C. Baker, Starfire, a commercial tokamak power plant, Nucl. Eng. Des. 63 (1981) 199–231.
[69] C.D. Henning, B.G. Logan, Overview of tiber-II—Evolution toward an engineering test reactor, J. Fusion Energy 6.3 (1987) 241–256.
[70] C.D. Henning, J.R. Gilleland, Tiber II as a precursor to an international thermonuclear experimental reactor, Fusion Eng. Des. 8 (1989) 37–42.
[71] F. Najmabadi, et al., The ARIES-I Tokamak Reactor Study, Univ. of California at Los Angeles, CA, 1991. Final Report, 1991, Rep. UCLA-PPG-1323.
[72] F. Najmabadi, A Team, Spherical torus concept as power plants–the ARIES-ST study, Fusion Eng. Des. 65 (2003) 143–164.
[73] F. Najmabadi, et al., The ARIES-AT advanced tokamak, advanced technology fusion power plant, Fusion Eng. Des. 80 (2006) 3–23.
[74] D.M. Meade, Fusion ignition research experiment (FIRE), Fusion Technol. 39.2P2 (2001) 336–342.
[75] C.E. Kessel, et al., Overview of the fusion nuclear science facility, a credible break-instep on the path to fusion energy, Fusion Eng. Des. 135 (2018) 236–270.
[76] Y.K.M. Peng, et al., Fusion Nuclear Science Facility (FNSF), in: Proceedings of the IEEE/NPSS 24th Symposium on Fusion Engineering, IEEE, 2011.
[77] B.N. Sorbom, ARC: a compact, high-field, fusion nuclear science facility anddemonstration power plant with demountable magnets, Fusion Eng. Des. 100 (2015) 378–405.
[78] A. Sykes, et al., Compact fusion energy based on the spherical tokamak, Nucl. Fusion 58.1 (2017) 016039.
[79] M. Kikuchi, Steady state tokamak reactor based on the bootstrap current, Nucl. Fusion 30.2 (1990) 265.
[80] S. Nishio, K. Tobita, K. Ushigusa, S. Konishi, R.D. Team, Conceptual design of tokamak high power reactor (A-SSTR2), J. Plasma Fusion Res. 78 (11) (2002) 1218–1230.
[81] T. Ando, S. Nishio, H. Yoshimura, Design of the high-T/sub c/superconducting TF coil for the tight aspect ratio Tokamak power reactor (VECTOR), IEEE Trans. Appl. Supercond. 14.2 (2004) 1481–1484.
[82] K. Tobita, et al., SlimCS—compact low aspect ratio DEMO reactor with reduced-size central solenoid, Nucl. Fusion 47.8 (2007) 892.
[83] S. Nishio, K. Tobita, S. Konishi, T. Ando, S. Hiroki, T. Kuroda, M. Yamauchi, M. Azumi, Tight aspect ratio tokamak power reactor with superconducting TF coils, No JAERI-REVIEW–2003-011 (2003).
[84] R Stambaugh, V Chan, R Miller, M Schaffer, The spherical tokamak route to fusion power' fusion, Technology 33 (1998) p1.
[85] A. Sykes, et al., The spherical Tokamak path to fusion power—Revisited, in: Proceedings of the IEEE 25th Symposium on Fusion Engineering (SOFE), IEEE, 2013.
[86] O. Mitarai, Y. Takase, Plasma current rampup by the outer vertical field coils in a spherical tokamak reactor, Fusion Sci. Technol. 43.1 (2003) 67–90.
[87] P.F. Buxton, M.P. Gryaznevich, Merging compression start-up predictions for ST40, Fusion Eng. Des. 123 (2017) 551–554.
[88] P.H. Titus, C. Kessel, FNSF structural sizing studies, Fusion Sci. Technol. 77 (2021) 7–8, 557-567.
[89] A.J. Wootton, et al., Compact Tokamak Reactors. Part 1 (analytic results). No. DOE/ER/54241-163; FRCR-484, Univ. of Texas, Austin, TX (United States), 1996.
[90] P. Barabaschi, S. Chiocchio, ITER: the design basis and challenges ahead, in: Proceedings of the 20th IEEE/NPSS Symposium on Fusion Engineering. S. Diego (CA), Oct 2003.
[91] E. Fable, et al., Plasma physics for fusion reactor system codes: framework and model code, 2018, Fusion Eng. Des. 130 (2018) 131. May.
[92] E. Fable, et al., Novel free-boundary equilibrium and transport solver with theory-based models and its validation against ASDEX Upgrade current ramp scenarios, Plasma Phys. Control Fusion 55.12 (2013) 124028.
[93] Romanelli, F, et al. "Fusion electricity: a roadmap to the realization of fusion energy." (2012).
[94] C. Bachmann, Conceptual study of the remote maintenance of the DEMO breeding blanket, Fus. Eng. Des. 177 (2022) 113077.
[95] M.R. Gilbert, et al., Waste assessment of European DEMO fusion reactor designs, Fusion Eng. Des. 136 (2018) 42–48.
[96] S.M.G. de Vicente, et al., Overview on management of radioactive wastes from fusion facilities: ITER, DEMOnstration machines and power plants, Nucl. Fusion (2022).
[97] R. Wenninger, et al., Advances in the physics basis for the European DEMO design, Nucl. Fusion 55.6 (2015) 063003.
[98] M.A. Abdou, D.A. Ehst, L.M. Waganer, Results of Systems Studies For the STARFIRE Commercial Tokamak. No. CONF-791102-126, Argonne National Lab., IL (USA); McDonnell Douglas Astronautics Co., St. Louis, MO (USA), 1979.
[99] R.D. Stambaugh, L.L. Lao, E.A. Lazarus, Relation of vertical stability and aspect ratio in tokamaks, Nucl. Fusion 32.9 (1992) 1642.
[100] H. Zohm, Magnetohydrodynamic Stability of Tokamaks, John Wiley & Sons, 2015.
[101] M. Wilson, Superconducting Magnets, Oxford University Press, 1983. ISBN 978-0-19-854810-2.
[102] M. Kovari, et al., PROCESS": a systems code for fusion power plants—part 1: physics, Fusion Eng. Des. 89.12 (2014) 3054–3069.
[103] M. Mattei, et al., ITER operational space for full plasma current H-mode operation, Fusion Eng. Des. 84.2-6 (2009) 300–304.
[104] R Albanese, et al., Electromagnetic analyses of single and double null configurations in DEMO device, Fusion Eng. Des. 146 (2019) 1468–1472.
[105] M. Huguet, ITER Home Teams, Key engineering features of the ITER-FEAT magnet system and implications for the R&D programme, Nucl. Fusion 41.10 (2001) 1503.
[106] X. Sarasola, et al., Progress in the design of a hybrid HTS-Nb 3 Sn-NbTi central solenoid for the EU DEMO, IEEE Trans. Appl. Supercond. 30.4 (2020) 1–5.
[107] R. Wesche, et al., Central solenoid winding pack design for DEMO, Fusion Eng. Des. 124 (2017) 82–85.
[108] A. Di Zenobio, et al., DTT device: conceptual design of the superconducting magnet system, Fusion Eng. Des. 122 (2017) 299–312.
[109] M. Verrecchia, et al., ITER-FEAT central solenoid structural analysis and fatigue life assessment, Fusion Eng. Des. 58 (2001) 141–146.
[110] N. Mitchell, et al., The ITER magnets: design and construction status, IEEE Trans. Appl. Supercond. 22.3 (2011), 4200809-4200809.
[111] K. Hamada, et al., Demonstration of full scale JJ1 and 316LN fabrication for ITER TF coil structure, Fusion Eng. Des. 82.5-14 (2007) 1481–1486.
[112] Hull, J.R., et al. "Superconducting magnets." Applied Superconductivity: Handbook on Devices and Applications (2015): 403–602.
[113] Gray, W. H., Stoddart W. C.T., and Akin J. E.. Bending free toroidal shells for tokamak fusion reactors. No. CONF-771029-145. Oak Ridge National Lab., Tenn. (USA); Tennessee Univ., Knoxville (USA), 1977.

[114] C.G. Windsor, et al., Tungsten boride shields in a spherical tokamak fusion power plant, Nucl. Fusion 61.8 (2021) 086018.
[115] J.L. Duchateau, et al., Conceptual design for the superconducting magnet system of a pulsed DEMO reactor, Fusion Eng. Des. 88 (2013) 1609–1612.
[116] J.B Hicks, Toroidal field system for tight aspect ratio tokamak reactors, Fusion Eng. Des. 18 (1991) 227–232.
[117] Mendelssohn, K. "Quest for absolute zero: the meaning of low temperature physics." (1977).
[118] C. Bachmann, Overview over DEMO design integration challenges and their impact on component design concepts, Fusion Eng. Des. 136 (2018) 87–95.
[119] A. Del Nevo, et al., Recent progress in developing a feasible and integrated conceptual design of the WCLL BB in EUROfusion project, Fusion Eng. Des. 146 (2019) 1805–1809.
[120] F.A. Hernandez, et al., An enhanced, near-term HCPB design as driver blanket for the EU DEMO, Fusion Eng. Des. 146 (2019) 1186–1191.
[121] P. Pereslavtsev, Neutronic analyses of generic issues affecting the tritium breeding performance in different DEMO blanket concepts, Fusion Eng. Des 109–111 (2016) 1067–1768.
[122] T. Eich, et al., Inter-ELM power decay length for JET and ASDEX Upgrade: measurement and comparison with heuristic drift-based model, Phys. Rev. Lett. 107.21 (2011) 215001.
[123] T. Eich, et al., Scaling of the tokamak near the scrape-off layer H-mode power width and implications for ITER, Nucl. Fusion 53.9 (2013) 093031.
[124] M. Greenwald, et al., A new look at density limits in tokamaks, Nucl. Fusion 28.12 (1988) 2199.
[125] M. Siccinio, et al., Figure of merit for divertor protection in the preliminary design of the EU-DEMO reactor, Nucl. Fusion 59.10 (2019) 106026.
[126] Ch Bachmann, et al., Issues and strategies for DEMO in-vessel component integration, Fusion Eng. Des. 112 (2016) 527–534.
[127] C. Bachmann, et al., Containment structures and port configurations, Fusion Eng. Des. 174 (2022) 112966.
[128] L. Giannini, et al., The MAgnet Design Explorer algorithm (MADE) for LTS, hybrid or HTS toroidal and poloidal systems of a tokamak with a view to DEMO, Fusion Eng. Des. 193 (2023) 113659.
[129] J.L. Duchateau, et al., Conceptual integrated approach for the magnet system of a tokamak reactor, Fusion Eng. Des. 89.11 (2014) 2606–2620.